

Homoleptic Phosphino Copper(I) Complexes with in Vitro and in Vivo Dual Cytotoxic and Anti-angiogenic Activity

V. Gandin,^{a†} A. Trenti,^{a†} M. Porchia,^b F. Tisato,^b M. Giorgetti,^c I. Zanusso,^a L. Trevisi^a and C. Marzano^{a*}

^a Dipartimento di Scienze del Farmaco, Università di Padova, via Marzolo 5, 35131 Padova, Italy.

^b IENI-CNR, Corso Stati Uniti 4, 35127 Padova, Italy

^c Dipartimento di Chimica Industriale, Università di Bologna, Viale Risorgimento 4, 40136 Bologna, Italy

†these authors contributed equally

Characterization of complex $[\text{Cu}(\text{DAPTA})_4][\text{BF}_4]$, **2**

Figure S1. IR spectrum of **2** in KBr pellets

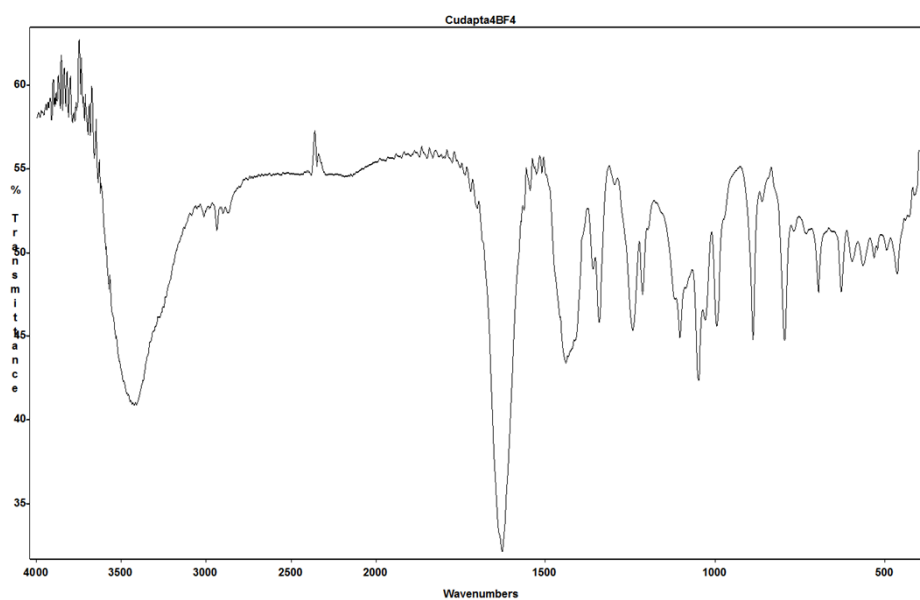


Figure S2. $^{31}\text{P}\{^1\text{H}\}$ NMR spectrum of **2** in CD_3CN solution

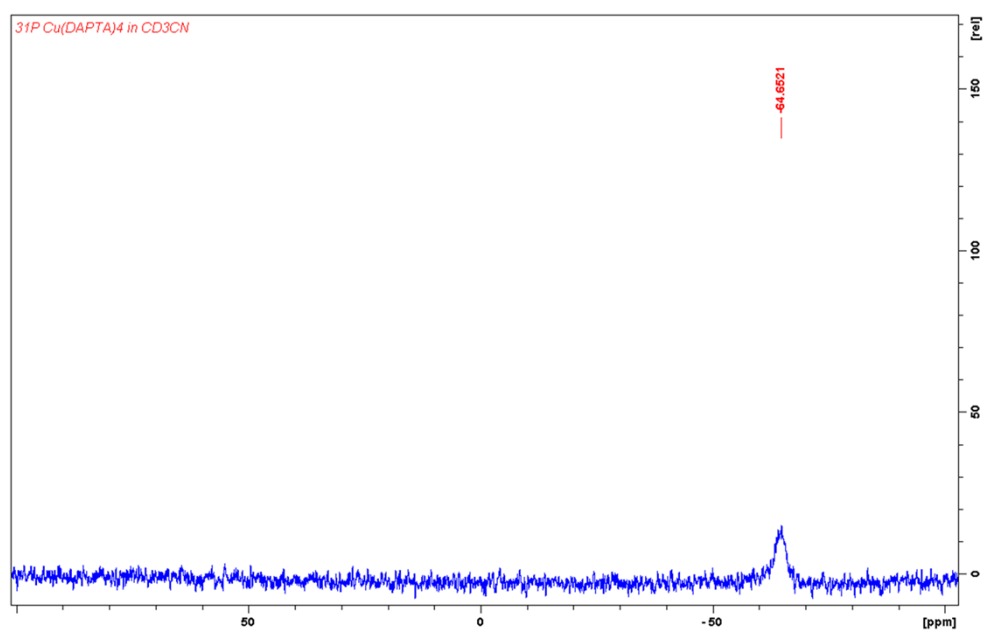


Figure S3. $^{13}\text{C}\{^1\text{H}\}$ NMR spectrum of **2** in CD_3CN solution in the 0 – 100 ppm region

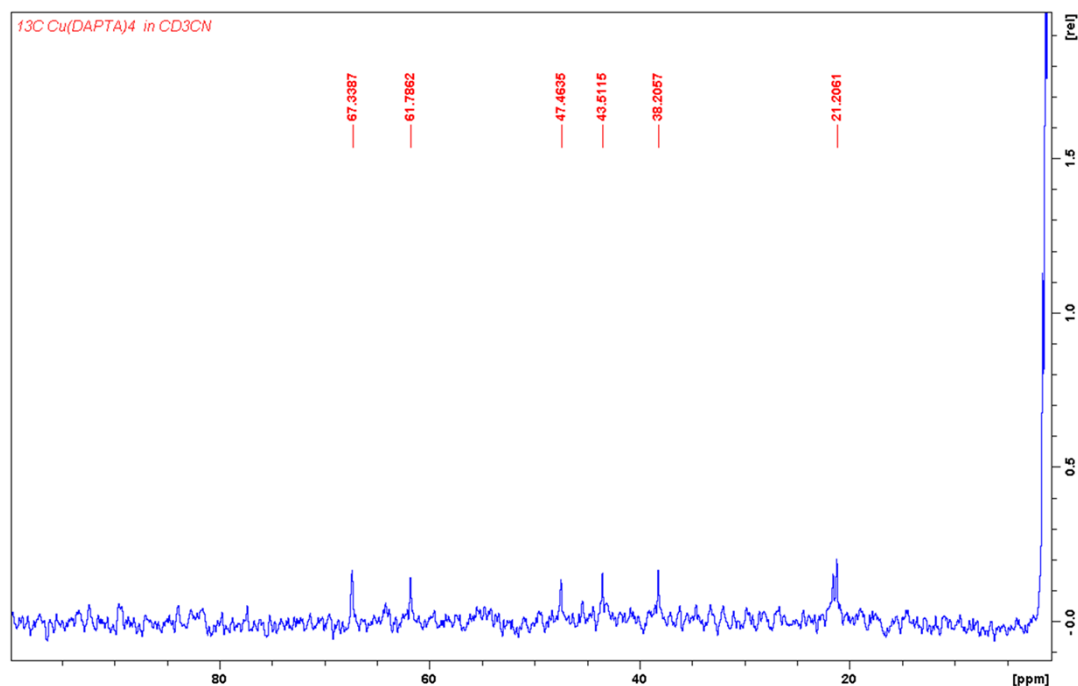
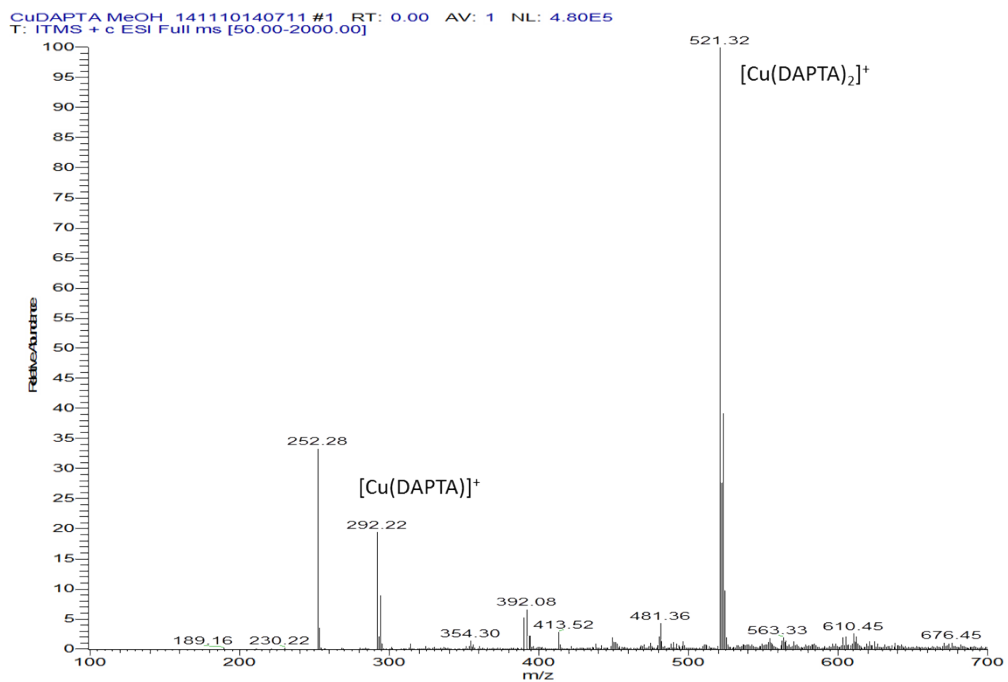


Figure S4. Full ESI(+)-MS spectrum of **2**, in MeOH solution.



Characterization of complex $[\text{Cu}(\text{PTA-SO}_2)_4][\text{BF}_4]$, **3**

Figure S5. IR spectrum of **3** in KBr pellets

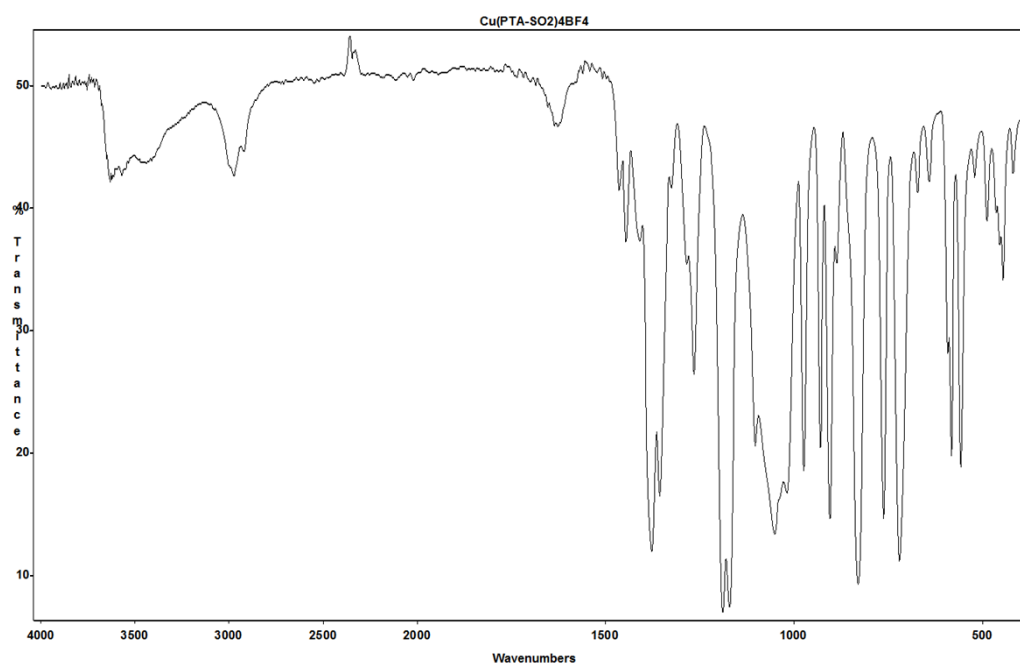


Figure S6. ¹H NMR spectrum of **3** in DMSO-d₆ solution

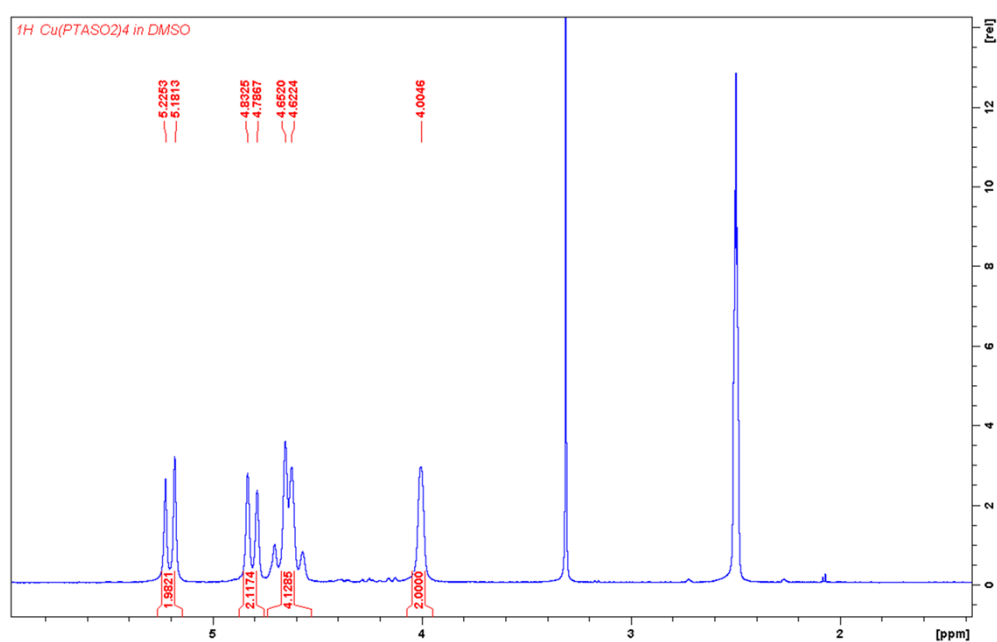


Figure S7. $^{31}\text{P}\{^1\text{H}\}$ NMR spectrum of **3** in DMSO- d_6 solution

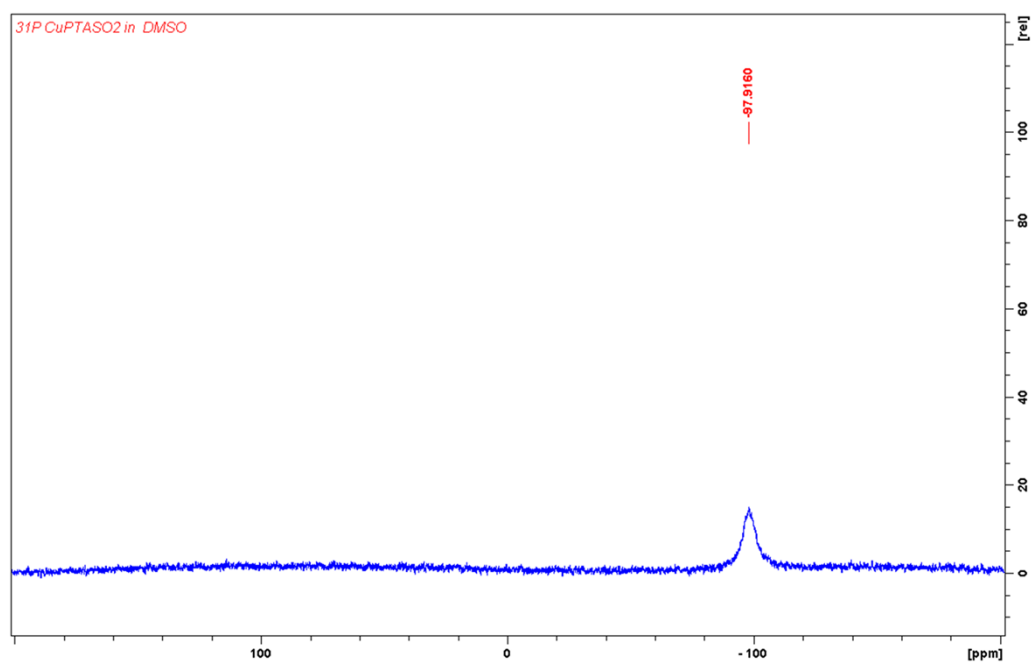


Figure S8. $^{13}\text{C}\{^1\text{H}\}$ NMR spectrum of **3** in DMSO- d_6 solution in the 0 – 100 ppm region

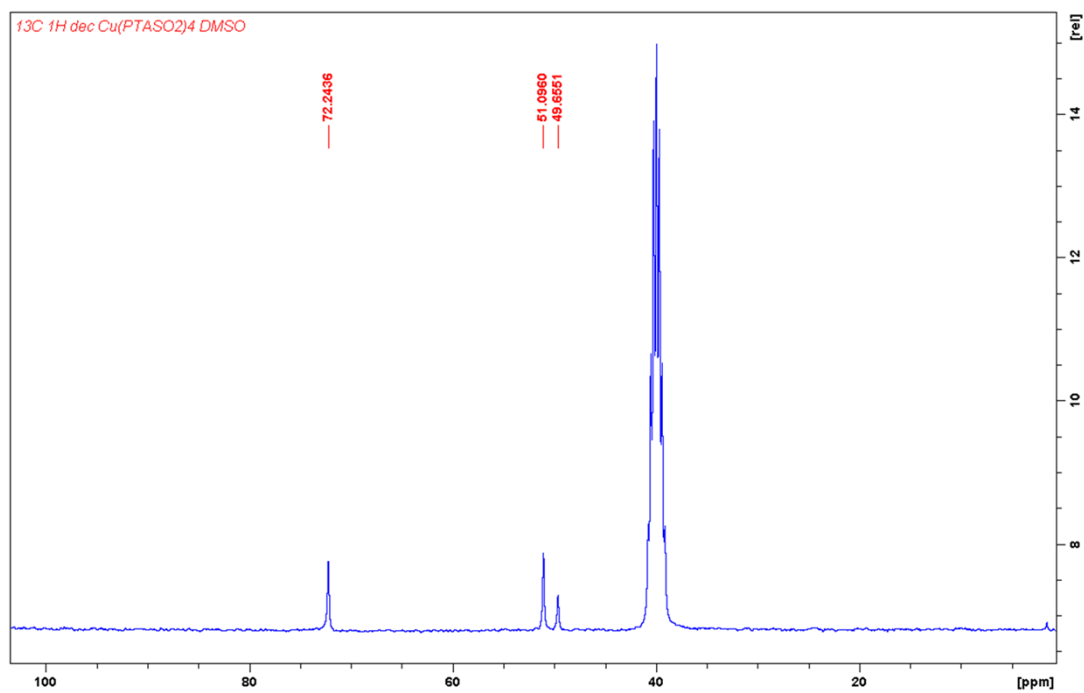


Figure S9. Full ESI(+)-MS spectra of the complex $[\text{Cu}(\text{PTA-SO}_2)_4][\text{BF}_4]$, **3** in DMSO/MeOH solution.

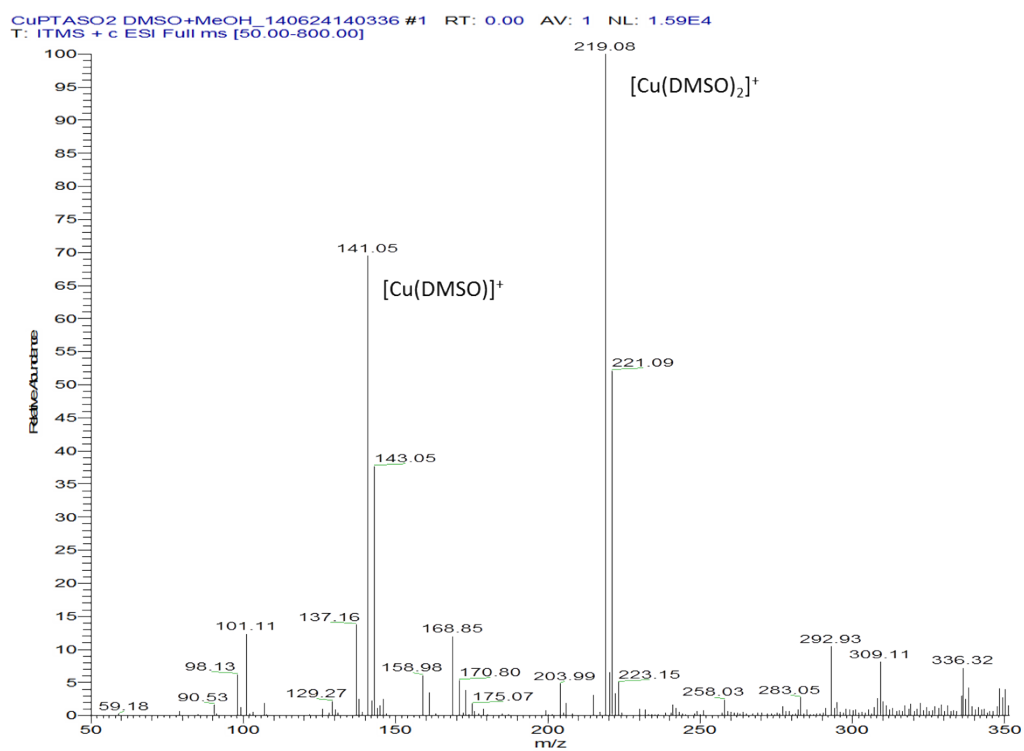
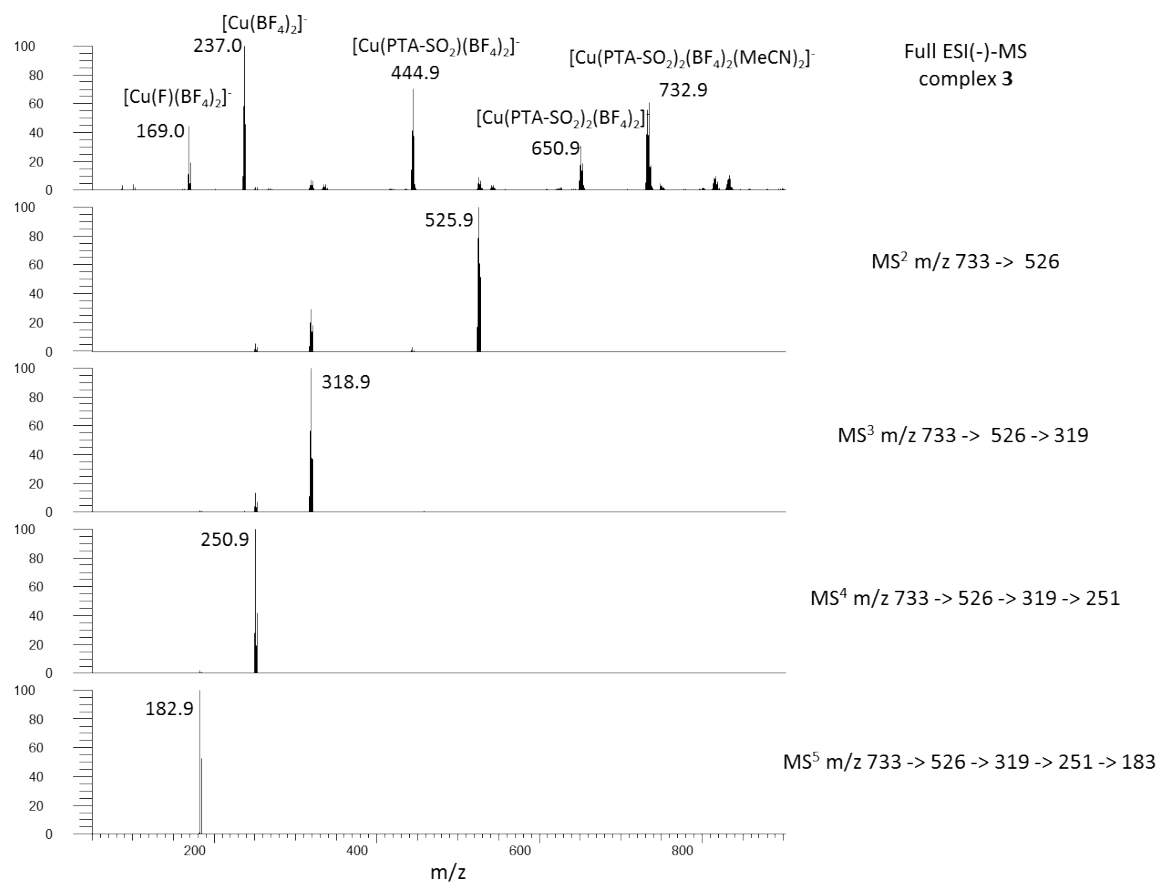


Figure S10. Full ESI(-)-MS spectra of the complex $[\text{Cu}(\text{PTA-SO}_2)_4][\text{BF}_4]$, **3** in MeCN solution, and collisionally induced decomposition (MS^n) of the rearranged ion $[\text{Cu}(\text{PTA-SO}_2)_2(\text{BF}_4)_2(\text{MeCN})_2]^-$ at m/z 733.



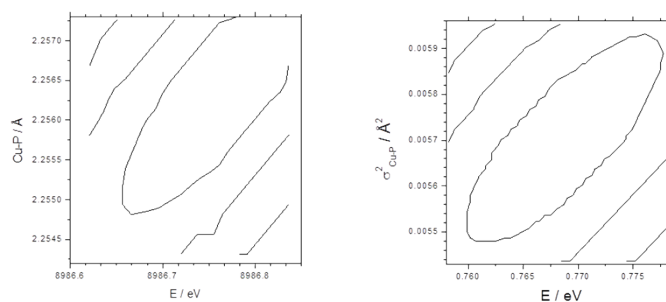
XAS data Analysis

XAS data analysis. X-Ray absorption near edge structure (XANES) spectrum was normalized to an edge jump of unity. A prior removal of the background absorption was done by subtraction of a linear function extrapolated from the pre-edge region. The EXAFS analysis was performed with the GNXAS package^{1,2} that takes into account the Multiple Scattering (MS) theory. The method is based on the decomposition of the EXAFS signals into a sum of several contributions, that are the n-body terms. It allows the direct comparison of the raw experimental data with a model theoretical signal. The procedure avoids any filtering of the data and allows a statistical analysis of the results. The theoretical signal is calculated *ab-initio* and contains the relevant two-body $\gamma^{(2)}$ and the three-body $\gamma^{(3)}$ multiple scattering (MS) terms. The phase shifts for the photoabsorber and backscatterer atoms were calculated *ab-initio* using a suitable structural model, in the muffin-tin approximation. The structural model was based on the crystal structure (coordinates) for DAPTA ligand available in the paper by Darensbourg. [ENREF 3](#)³ Referring to the structure of DAPTA, the following n-body terms have been included in the fitting procedures: the two-atom contributions $\gamma^{(2)}$ Cu-P with degeneracy of 4, the three-body contributions $\eta(3)$ Cu-P-C with degeneracy of 12 (from four DAPTA ligands). It is noteworthy that the inclusion of the three-body term $\eta(3)$ allows monitoring the shells beyond the first one by using the same three-atom coordinates both for the two-atom and the three-atom contributions. For instance, the three-body signal $\eta(3)$ Cu-P-C includes both $\gamma^{(2)}$ Cu--C and $\gamma^{(3)}$ Cu-P-C contributions. Data analysis has been performed by minimizing a χ^2 -like function that compares the theoretical model to the experimental signal. The Hedin-Lundqvist complex potential was used for the exchange-correlation potential of the excited state. The core hole lifetime, Γ_c , was fixed to the tabulated value and included in the phase shift calculation. The experimental resolution used in the fitting analysis was about 2 eV, in agreement with the stated value for the beamline used. The E_0 value was found to be displaced by several eV with respect to the edge inflection point, 8986.7(3) eV and the value of S_0^2 to be 0.77(2). The total number of parameters taken into account in the fitting procedure (including the structural and non-structural terms E_0 , S_0^2 and the experimental resolution) is 10, whereas the number of floating variable (fitting) was found to be 8. Besides, it is worth mentioning that in all cases the number of fitting parameters does not exceed the estimated 'number of independent data points' $N_{ind} = (2\delta k \delta R / \pi) + 2$, ensuring that the fit is well determined, thus confirming the reliability of the minimization.

Table S1. EXAFS fitting results for complex **2**. The estimated parameter errors are indicated in parentheses

Bond length (degeneracy)	complex 2
Debye Waller Factor	
Cu-P/ Å (4)	2.256(2)
σ^2 / Å ²	0.0057(3)
Cu-P-C / deg (9)	123(3)
σ^2_{θ} / deg ²	77(10)
P-C/ Å	1.78(2)
σ^2 / Å ²	0.008(3)
E_0 , eV	8986.7(3)
S_0^2	0.77(2)

Figure S11. Examples of CONTOUR plot for complex **2** for the error parameters determination. These plots were selected among the parameters having strongest correlation to reflect the highest error. The estimated statistical error is associated with the 95% confidence interval.



REFERENCES

1. A. Filipponi, *Journal of Physics-Condensed Matter*, 1995, 7, 9343-9356.
2. A. Filipponi, A. DiCicco and C. R. Natoli, *Physical Review B*, 1995, 52, 15122-15134.
3. D. J. Darensbourg, C. G. Ortiz and J. W. Kamplain, *Organometallics*, 2004, 23, 1747-1754.

